relative to troilite in the meteorite Canyon Diablo) indicate that the sulfuric acid responsible for cave genesis was derived from biogenic hydrogen sulfide (*4, 9, 10*) most likely produced at the base of the Castile Formation in the Delaware Basin immediately south of the Guadalupe Mountains (*9*). The caves were formed when the hydrogen sulfide was oxidized to sulfuric acid as it migrated upward and approached the water table in the Capitan reef and forereef facies (Capitan Limestone) (*9*); massive amounts of limestone and dolostone were subsequently dissolved or replaced by gypsum.

9. C. A. Hill, *Geology of the Delaware Basin, Guadalupe, Apache, and Glass Mountains, New Mexico and West Texas*, Permian Basin Section, SEPM Publ. 96-39 (Society for Sedimentary Geology, Tulsa, OK, 1996).
10. V. J. Polyak and N. Güven, *Clays Clay Mineral.* **44**, 843 (1996); V. J. Polyak and P. Provencio, *J. Caves Karst Studies*, in press.
11. R. P. Ashley and M. L. Silberman, *Econ. Geol.* **71**, 904 (1976); P. G. Vikre, *ibid.* **80**, 360 (1985).
12. M. I. Bird, A. R. Chivas, I. McDougall, *ibid. (Isotope Geosci. Sect.).* **80**, 133 (1990); G. B. Arehart, S. E. Kesler, J. R. O'Neil, K. A. Foland, *ibid.* **87**, 263 (1992); P. M. Vasconcelos, G. H. Brimhall, T. A. Becker, P. R. Renne, *Geochim. Cosmochim. Acta* **58**, 401 (1994).
13. D. C. Ford and C. A. Hill, *Isochron/west* **54**, 3 (1989).
14. Supplementary details of $^{40}Ar/^{39}Ar$ analytical procedures, irradiation parameters, and tables of results for individual analyses are available at www.sciencemag.org/feature/data/976753.shl. In summary, samples were irradiated in vacuo with interlaboratory standard Fish Canyon Tuff sanidine as a neutron fluence monitor: FCT-1 with an age of 27.84 Ma [A. Deino and R. Potts, *J. Geophys. Res.* **95**, 8453 (1990)] relative to a Mmhb-1 flux monitor at 520.4 Ma [S. D. Samson and E. C. Alexander, *Chem. Geol. (Isotope Geosci. Sect.).* **66**, 27 (1987)]. J factors were determined by CO_2 laser-fusion analyses to a precision of ±0.15 to 0.25% (±2 sigma). Alunite aliquots (15 to 50 mg) were incrementally heated in a double-vacuum molybdenum resistance furnace in 7 to 10 steps at temperatures of 500° to 750°C. Isotopic compositions of argon were measured with a Mass Analyzer Products model 215-50 mass spectrometer. Decay constants and isotopic abundances used in calculations are those suggested by R. H. Steiger and E. Jäger [*Earth Planet. Sci. Lett.* **36**, 359 (1977)]. Plateau ages and associated uncertainties for samples with flat age spectra, defined by two or more contiguous incremental steps that comprised >50% of total ^{39}Ar released and agreed in age within 2 standard deviations, were calculated by using the error formula of S. D. Samson and E. C. Alexander [*Chem. Geol. (Isotope Geosci. Sect.)* **66**, 27 (1987)].
15. T. C. Onstott, M. L. Miller, R. C. Ewing, G. W. Arnold, D. S. Walsh, *Geochim. Cosmochim. Acta* **59**, 1821 (1995); D. York, N. M. Evenson, P. E. Smith, *U.S. Geol. Surv. Circ.* **1107**, 360 (1994).
16. R. E. Stoffregen, R. O. Rye, M. D. Wasserman, *Geochim. Cosmochim. Acta* **58**, 917 (1994).
17. T. Itaya, A. Arribas Jr., T. Okada, *ibid.* **60**, 4525 (1996).
18. G. E. Hendrickson and R. S. Jones, *Geology and Ground-Water Resources of Eddy County, New Mexico* (New Mexico Bureau of Mines and Mineral Resources Groundwater Report 3, Socorro, NM, 1952); W. S. Motts, *Geol. Soc. Am. Bull.* **79**, 283 (1968); W. L. Hiss, *N.M. Geol. Soc. Guidebook* **31**, 289 (1980); H. R. DuChene and J. S. McLean, in *Subsurface and Outcrop Examination of the Capitan Shelf Margin, Northern Delaware Basin*, P. M. Harris and G. A. Grover, Eds. (SEPM Core Workshop 13, San Antonio, TX, 1989), p. 475.
19. G. A. Izett, *Geol. Soc. Am. Mem.* **144**, 179 (1975); W. E. Elston, *Tectonics* **3**, 229 (1984); G. P. Eaton in *Continental Extensional Tectonics*, M. P. Coward, J. F. Dewey, P. L. Hancock, Eds. (Geological Society Special Publication 28, Blackwell, Oxford, 1987), p. 355; D. S. Barker, *Geol. Soc. Am. Bull.* **88**, 1421 (1977); J. S. Compton, S. W. Snyder, D. A. Hodell, *Geology* **18**, 1227 (1990); P. Cabezas, *N.M. Geol.* **13**, 25 (1991); C. E. Chapin and S. M. Cather, *Geol. Soc. Am. Spec. Pap.* **291**, 5 (1994).
20. B. P. Flower and J. P. Kennett, *Palaeogeogr. Palaeoclimatol. Palaeoecol.* **108**, 537 (1994); J. A. Wolfe, *ibid.*, p. 195; C. Latorre, J. Quade, W. C. McIntosh, *Earth Planet. Sci. Lett.* **146**, 83 (1997); G. M. Filippelli, *Geology* **25**, 27 (1997).
21. We thank C. E. Chapin of the New Mexico Bureau of Mines and Mineral Resources, Socorro, New Mexico; D. C. Ford of McMaster University, Hamilton, Ontario, Canada; and C. A. Hill, consulting geologist, Albuquerque, NM, for their prereview of this paper. We thank D. Pate, J. Richards, and the Carlsbad Caverns National Park Service; J. Goodbar and the Carlsbad District Bureau of Land Management; and R. Turner and the Lincoln National Forest Service for the necessary permits and field assistance. Funding for the $^{40}Ar/^{39}Ar$ geochronology work was provided by the New Mexico Bureau of Mines and Mineral Resources.

16 December 1997; accepted 5 February 1998

Partial Hormone Resistance in Mice with Disruption of the Steroid Receptor Coactivator-1 (SRC-1) Gene

Jianming Xu, Yuhong Qiu, Francesco J. DeMayo, Sophia Y. Tsai, Ming-Jer Tsai, Bert W. O'Malley*

The in vivo biological function of a steroid receptor coactivator was assessed in mice in which the SRC-1 gene was inactivated by gene targeting. Although in both sexes the homozygous mutants were viable and fertile, target organs such as uterus, prostate, testis, and mammary gland exhibited decreased growth and development in response to steroid hormones. Expression of RNA encoding TIF2, a member of the SRC-1 family, was increased in the SRC-1 null mutant, perhaps compensating partially for the loss of SRC-1 function in target tissues. The results indicate that SRC-1 mediates steroid hormone responses in vivo and that loss of its coactivator function results in partial resistance to hormone.

Sex steroid hormones have central roles in the control of puberty, sexual behavior, and reproductive functions. Their receptors belong to the nuclear receptor superfamily of ligand-dependent transcription factors (*1, 2*). Upon hormone binding, steroid receptors undergo conformational change, bind to their cognate DNA response elements on nuclear target genes, and recruit coactivators and general transcription factors (GTFs) to form an active transcriptional complex, resulting in site-directed chromatin remodeling and enhancement of target gene expression (*1, 3–8*). SRC-1 is a coactivator for the steroid receptor superfamily; it functions in transcriptional activation through its histone acetyltransferase activity (HAT) and multiple interactions with agonist-bound receptors, other coactivators such as CBP or P300, other HAT such as p/CAF, and some GTFs such as TBP and TIFIIB (*7, 9–11*). SRC-1 is a member of a gene family that includes SRC-1, TIF2 (also termed GRIP-1 and SRC-2), and p/CIP (also termed RAC3, ACTR, AIB1, and SRC-3) (*6, 9–16*). Cell-free and in vitro transcription experiments have indicated that the SRC-1 family members enhance receptor-dependent transactivation of nuclear genes (*6, 9–16*). AIB1 is amplified and overexpressed in many breast cancers and thus could have a role in tumorigenesis (*16*).

To dissect the physiological role of SRC-1 in vivo, we used gene targeting to disrupt the endogenous SRC-1 gene in embryonic stem (ES) cells. The targeting vector contained 3.5-kb (5′) and 2.5-kb (3′) mouse SRC-1 genomic sequences flanking a GLVP cassette (*17*) and a neomycin-resistance gene (PGK-*neo*) (Fig. 1A). In addition, the herpes simplex virus thymidine kinase (HSV-TK) gene was located outside of the SRC-1 sequence and served as a negative drug-selection marker. After correct recombination, the targeting event inserted an in-frame stop codon at the Met^{381} position and deleted ~9 kb of genomic sequence extending downstream of Met^{381}. Because the oligonucleotide sequence corresponding to Asp^{816} to Thr^{826} was detected in an Eco RV–Xba I fragment within the 9-kb region, targeting deleted the SRC-1 exon sequence encoding at least 446 amino acids (Met^{381} to Thr^{826}). Except for the NH_2-terminal basic helix-loop-helix and Per-Arnt-Sim (bHLH-PAS) domains, all SRC-1 functional domains for transcriptional activation, HAT activity, and interactions with nuclear receptors CBP, P300, and p/CAF were disrupted by the targeting event (*6, 7, 9, 10, 14, 18*).

After electroporation and drug selection

Department of Cell Biology, Baylor College of Medicine, Houston, TX 77030, USA.

*To whom correspondence should be addressed. E-mail: berto@bcm.tmc.edu

with geneticin (G418) and FIAU (*19*), we identified 16 correctly targeted ES cell lines by Southern (DNA) analyses (Fig. 1, A and B). Three independent lines of chimeric founders were generated by microinjecting targeted ES cell lines into blastocysts donated from a C57 strain. We used two lines to inbreed with a 129Sv mouse strain and outbreed with a C57 strain to produce offspring. SRC-1 genotypic analyses by Southern blotting and polymerase chain reaction (PCR) confirmed that SRC-1–specific heterozygous and homozygous mutants were obtained (Fig. 1C). Heterozygotes appeared to be normal and were indistinguishable from wild-type mice. In homozygotes, both the 8.5- and the 6.5-kb SRC-1 mRNAs were absent when analyzed by Northern blot analysis (*20*). To confirm the absence of the COOH-terminus of SRC-1 protein in homozygotes, we used a monoclonal antibody (*7*) specific to the region of amino acids 840 to 947 in protein immunoblotting extracts prepared from kidney and liver. The SRC-1 protein was undetectable in assays with extracts from the homozygous mutant (Fig. 1D). Although the RNA encoding the bHLH-PAS domain was expressed in the mutants at a level similar to that in the wild-type mice (*20*), it would not have a dominant negative effect because this domain interacted with neither the full-length SRC-1 nor other SRC-1 family members such as TIF2 (*21*).

SRC-1 null mutants exhibited no obvious external phenotype. Both male and female homozygotes were fertile and showed growth rates similar to wild-type mice. We therefore examined steroid action in target organs including uterus, prostate, and mammary gland. Uterine response to mechanical traumatization (decidual stimulation) is a progesterone receptor (PR)–dependent process (*22*). We treated ovariectomized wild-type and mutant mice with a high dose of progesterone and a low dose of estrogen, followed by mechanical stimulation of the left uterine horn of each animal (*22*). The unstimulated right uterine horn served as a control. The decidual response, exhibited as an increase in uterine horn size, was consistently observed in the stimulated left uterine horn in wild-type mice, but the uterine horn of the SRC-1 null mutant revealed only a partial response (Fig. 2, A and B). We also examined estrogen-induced uterine growth in SRC-1 null mutants. Wild-type mice responded to estrogen treatment with a 4.3-fold increase in uterine wet weight. Uteri of homozygous SRC-1 mutants showed a smaller increase of about 2.8-fold (Fig. 2C). Thus, SRC-1 appears to be required for maximal uterine response to steroid hormone in vivo.

To assess androgen receptor function, we measured prostate growth in castrated male mice after they were treated with androgen. Eight days after castration, prostates in both wild-type and mutant mice regressed. Injection of testosterone for 7 days stimulated prostate growth in wild-type animals; a smaller response was observed in SRC-1

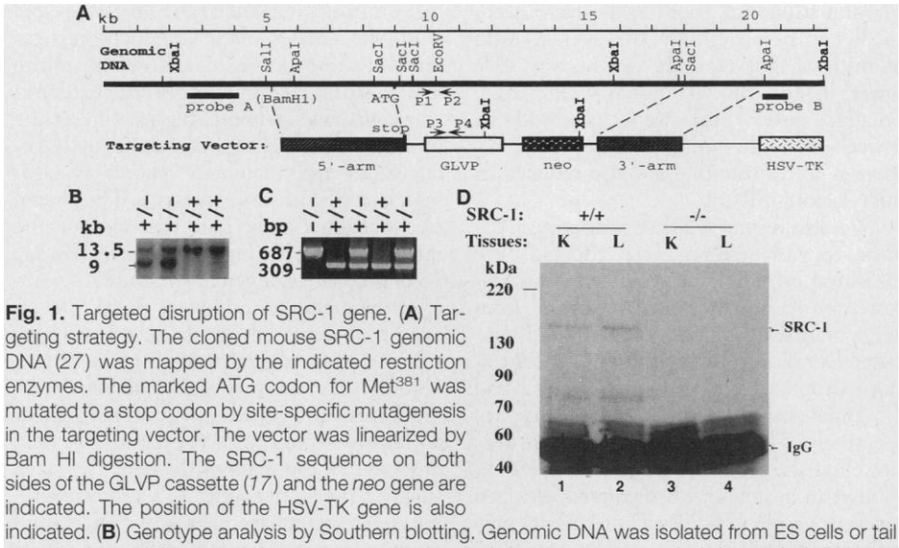

Fig. 1. Targeted disruption of SRC-1 gene. (**A**) Targeting strategy. The cloned mouse SRC-1 genomic DNA (*27*) was mapped by the indicated restriction enzymes. The marked ATG codon for Met^{381} was mutated to a stop codon by site-specific mutagenesis in the targeting vector. The vector was linearized by Bam HI digestion. The SRC-1 sequence on both sides of the GLVP cassette (*17*) and the *neo* gene are indicated. The position of the HSV-TK gene is also indicated. (**B**) Genotype analysis by Southern blotting. Genomic DNA was isolated from ES cells or tail samples from wild-type (+/+), homozygous mutant (−/−), or heterozygous (+/−) mice (*19*). DNA (15 μg) was digested by Xba I (A) and separated in a 0.7% agarose gel. The blot was analyzed by the 5′ probe A. The same blot was also analyzed by the 3′ probe B and the neo probe. (**C**) Genotype analysis by PCR. The same genomic DNA was used for the PCR template. The locations of specific primers (P1 to P4) are indicated in (A). The paired primers P1 (5′-caaccagcaaaggctgagtcca) and P2 (5′-agtacctc-ctgaggggttagag) detect a 309–base pair exon region that represents wild-type SRC-1. Primers P3 (5′-tgccgacgcgctagacgatttc) and P4 (5′-acacagcaaagaactggaggtg) detect a 687–base pair fragment located in the GLVP cassette, which represents the targeted SRC-1 locus. Results from PCR were consistent with those from Southern blot analysis whenever the same samples were assayed by both methods. (**D**) Absence of SRC-1 protein in homozygotes. Whole tissue lysates were prepared by homogenizing kidney (K) and liver (L) in 1× reducing sample buffer for SDS–polyacrylamide gel electrophoresis (7.5% gel). The blot was analyzed with a monoclonal antibody to the activation domain of SRC-1 (*7*). The endogenous mouse immunoglobulin G (IgG) from the tissues was detected by the secondary antibody, goat antibody to mouse immunoglobulin G conjugated to horseradish peroxidase (Bio-Rad).

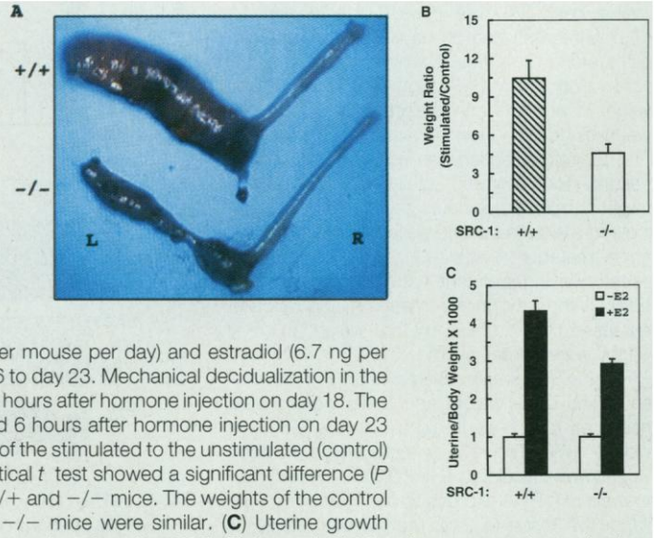

Fig. 2. Uterine responses in SRC-1 mutant mice. (**A** and **B**) Uterine response to a decidual stimulus. The decidual response was measured as described (*22*). Eight-week-old females (10 +/+ and 11 −/− animals) were ovariectomized on day 0, treated with estradiol (0.1 μg per mouse per day) from day 10 to day 12, and treated with progesterone (1 mg per mouse per day) and estradiol (6.7 ng per mouse per day) from day 16 to day 23. Mechanical decidualization in the left uterine horn was done 6 hours after hormone injection on day 18. The whole uterus was dissected 6 hours after hormone injection on day 23 (A). The ratio of the weights of the stimulated to the unstimulated (control) horn was calculated. Statistical *t* test showed a significant difference ($P < 0.01$) in the ratios from +/+ and −/− mice. The weights of the control horns from either +/+ or −/− mice were similar. (**C**) Uterine growth stimulated by estrogen assessed as described (*23*). Eight-week-old females were ovariectomized on day 0 and treated with estradiol (E2) (0.8 μg/kg/day) or sesame oil (solvent control) from day 15 to day 17. Uterine wet weight was measured on day 18. The ratio of uterine weight to body weight was calculated. The *t* test showed a significant difference ($P < 0.01$) in E2-treated +/+ ($n = 11$) and −/− ($n = 11$) uteri. Data in (B) and (C) represent two independent experiments (mean ± SEM).

mutant mice. The ratio of the weight of prostate and urethra to body weight revealed a 34% reduction in steroid-stimulated growth in the absence of SRC-1 (Fig. 3A). Although histological analysis did not reveal a structural disorder, the testes were smaller in homozygotes. The average ratio of testis weight to body weight was 19% lower in the SRC-1 mutants (Fig. 3B). Smaller testes also were observed in 3-week-old null mutants. Thus tissue responses to testosterone are also reduced in mice lacking SRC-1.

We also tested whether endocrine feedback control systems were affected. We measured estradiol, progesterone, and testosterone concentrations in serum from age-matched wild-type and SRC-1 null mutants. Estradiol and testosterone concentrations in female null mutants were 1.2 and 1.5 times those in wild-type animals, respectively. The SRC-1 null mutation does not elicit the typical hormonal changes exhibited in animals with disrupted estrogen receptor or PR (*22–24*). These results may reflect redundant coactivator function among multiple SRC-1 family members (*14*, *25*). Indeed, a twofold overexpression of TIF2 mRNA was detected in certain tissues such as brain and testis in SRC-1 null mutants, but expression of the p/CIP (RAC3) gene was unchanged (Fig. 3C). Thus TIF2 might compensate partially for the loss of SRC-1 in the null mutants.

Mammary development is tightly regulated by steroid hormones. Although prenatal morphogenesis of female mammary gland is relatively independent of steroid hormones, extensive growth of mammary gland during puberty requires estrogen. Physiologically, both estrogen and progesterone are essential for alveolar development during pregnancy (*26*). In 8-week-old wild-type females, mammary ducts grew extensively and occupied almost the entire mammary fat pad. In contrast, the extent of mammary ductal branching as well as the number of branches was substantially reduced in the mammary glands of age-matched SRC-1 null mutants. The ductal tree occupied only half the area of the mammary fat pad (Fig. 4, A and B). By day 18 of pregnancy, alveolar structures in wild-type mammary glands were highly developed and appeared on all ductal sections, filling the interductal spaces. In the SRC-1 mutant mammary glands, alveoli were much less developed in terms of number and size of alveoli, and very few alveoli were observed at the ends of ducts at the same stage of pregnancy (Fig. 4, C through F). Although mammary glands of SRC-1 null mutants can still produce milk, our results suggest that SRC-1 is required for normal mammary ductal elongation and alveolar development in vivo.

We also analyzed mammary gland development in response to estrogen and progesterone treatment in overiectomized adult mice. Estrogen and progesterone stimulate a complex ductal arborization and extensive alveolar formation in mammary glands of wild-type mice (*22*). This differentiated phenotype mimics a stage of mammary gland development in early pregnancy. In the mammary glands of SRC-1 mutant mice, only partial ductal growth was observed after hormone treatment (Fig. 4, G through J). Thus SRC-1 is required for efficient proliferation and differentiation of the mammary gland in response to estrogen and progesterone.

Our results demonstrate that a steroid receptor coactivator (SRC-1) is required for efficient steroid hormone action in vivo.

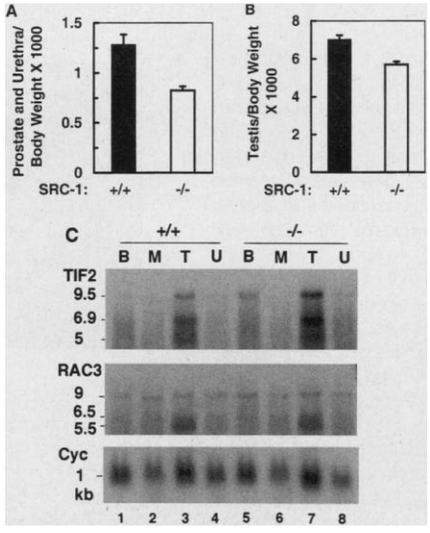

Fig. 3. Impaired response to testosterone in mice lacking SRC-1. (**A**) Stimulation of prostate growth. Twelve-week-old male mice (10 +/+ and 11 −/−) were castrated on day 0 and treated with testosterone (3 mg/kg/day) by subcutaneous injection during day 9 through day 15. The total weight of prostate and a section of urethra between bladder and penis was measured on day 16. The urethra section was included for technical reasons. Then the ratios of prostate and urethra weight to body weight were calculated. The *t* test showed a significant difference ($P < 0.01$) in hormone-treated +/+ and −/− mice. The data represent two independent experiments (mean ± SEM). Without hormone treatment, the ratios of regressed prostate and urethra weight to body weight were similar (~5.5×10^{-4}) in +/+ and −/− mice. (**B**) Smaller testes in SRC-1 null mutants. The body weight and testis weight were measured for 12-week-old male mice (23 +/+ and 19 −/−). The ratio of testis weight to body weight was calculated ($P < 0.01$ by *t* test). (**C**) Analysis of mRNA expression for TIF2 and p/CIP (RAC3). Total RNA (30 μg) from brains (B), mammary glands (M), testes (T), and uteri (U) of three +/+ or −/− mice was separated in each lane of the gel. Its blot was analyzed with ^{32}P-labled human TIF2 or RAC3 cDNA probes. Cyclophylin (Cyc) served as a control for RNA quantity. By densitometry, the density ratios of TIF2 RNA bands to the Cyc band were 0.27 (+/+) and 0.45 (−/−) for brains and 0.71 (+/+) and 1.34 (−/−) for testes. The density ratios of RAC3 RNA bands to the Cyc band were 0.20 (B), 0.33 (M), 0.41 (T) and 0.23 (U) for +/+, and 0.29 (B), 0.23 (M), 0.42 (T), and 0.31 (U) for −/−.

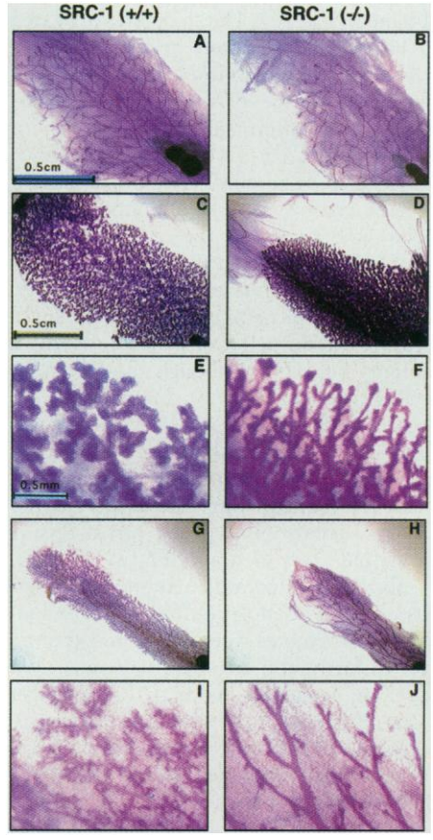

Fig. 4. Mammary gland development in SRC-1 null mutant mice. Whole mounts of mammary glands were prepared and stained as described (*22*). (**A** and **B**) The fourth pair of mammary glands from 8-week-old virgins with the indicated SRC-1 genotypes. (**C** and **D**) The fourth pair of mammary glands from mice pregnant for the first time with the indicated genotypes. (**E** and **F**) Higher magnification of the ducts and alveolar structures of the mammary glands in (C) and (D), respectively. (**G** and **H**) The fourth pair of mammary glands from 13-week-old females treated with progesterone and estradiol. Eight-week-old females were ovariectomized on day 0 and then treated with progesterone (1 μg per mouse per day) and estradiol (50 μg per mouse per day) from day 14 to day 34. Whole mounts of mammary glands were prepared on day 35. (**I** and **J**) Higher magnification of the mammary ducts and alveolar structures from (G) and (H), respectively. Scale bar in (A) also applies to (B); scale bar in (C) also applies to (D), (G), and (H); and scale bar in (E) also applies to (F), (I), and (J).

Loss of coactivation function in the SRC-1 null mutants may be partially compensated by increased expression of the closely related coactivator TIF2. Certain clinical syndromes of partial hormone resistance in which receptors are intact might be explained by impairment of nuclear receptor coactivators.

REFERENCES AND NOTES

1. M-J. Tsai nd B. W. O'Malley, *Annu. Rev. Biochem.* **63**, 451 (1994).
2. M. Beato, P. Herrlich, G. Schutz, *Cell* **83**, 851 (1995); D. J. Mangelsdorf *et al.*, *ibid.*, p. 835.
3. H. Shibata *et al.*, *Recent Prog. Horm. Res.* **52**, 141 (1997).
4. J. Wong, Y. B. Shi, A. P. Wolffe, *Genes Dev.* **9**, 2696 (1995).
5. A. P. Wolffe and D. Pruss, *Cell* **84**, 817 (1996).
6. H. Chen *et al.*, *ibid.* **90**, 569 (1997).
7. T. E. Spencer *et al.*, *Nature* **389**, 194 (1997).
8. G. Jenster *et al.*, *Proc. Natl. Acad. Sci. U.S.A.* **94**, 7879 (1997).
9. S. A. Onate, S. Y. Tsai, M-J. Tsai, B. W. O'Malley, *Science* **270**, 1354 (1995).
10. Y. Kamei *et al.*, *Cell* **85**, 403 (1996).
11. A. Takeshita *et al.*, *Endocrinology* **137**, 3594 (1996).
12. J. J. Voegel, M. J. S. Heine, C. Zechel, P. Chambon, H. Gronemeyer, *EMBO J.* **15**, 3667 (1996).
13. H. Hong, K. Kohli, A. Trivedi, D. L. Johnson, M. R. Stallcup, *Proc. Natl. Acad. Sci. U.S.A.* **93**, 4948 (1996).
14. J. Torchia *et al.*, *Nature* **387**, 677 (1997).
15. H. Li, P. J. Gomes, J. D. Chen, *Proc. Natl. Acad. Sci. U.S.A.* **94**, 8479 (1997).
16. S. L. Anzick *et al.*, *Science* **277**, 965 (1997).
17. The GLVP cassette encodes a transcriptional regulator composed of the activation domain of VP-16, the DNA binding domain of gal4, and the mutated ligand-binding domain of PR. This regulator can be activated only by a progesterone antagonist, RU-486 [Y. Wang, J. Xu, T. Pierson, B. W. O'Malley, S. Y. Tsai, *Gene Ther.* **4**, 432 (1997)]. This RU486-dependent transregulator could control a transgene containing a gal4-binding site. The GLVP regulator was incorporated in case the SRC-1 mutation resulted in a lethal phenotype.
18. D. M. Heery, E. Kalkhoven, S. Hoare, M. G. Parker, *Nature* **387**, 733 (1997).
19. Y. Qiu *et al.*, *Genes Dev.* **11**, 1925 (1997).
20. J. Xu, S. Y. Tsai, M.-J. Tsai, B. W. O'Malley, unpublished data.
21. T. E. Spencer, S. Y. Tsai, M-J. Tsai, B. W. O'Malley, unpublished data.
22. J. P. Lydon *et al.*, *Genes Dev.* **9**, 2266 (1995).
23. D. B. Lubahn *et al.*, *Proc. Natl. Acad. Sci. U.S.A.* **90**, 11162 (1993).
24. K. S. Korach *et al.*, *Recent Prog. Horm. Res.* **51**, 159 (1996).
25. C. L. Smith, S. A. Onate, M-J. Tsai, B. W. O'Malley, *Proc. Natl. Acad. Sci. U.S.A.* **93**, 8884 (1996).
26. Y. J. Topper and C. S. Freeman, *Physiol. Rev.* **60**, 1049 (1980).
27. Phage clones were identified by screening a 129Sv mouse genomic DNA library with a human SRC-1 cDNA probe. Inserts were excised by Not I digestion and subcloned into pBluescript II SK plasmid (Stratagene). Regions corresponding to specific amino acid sequences were defined by sequencing or by hybridization with oligonucleotide probes.

28. We thank K. Bramlett and L. A. Hadsell for technical assistance; C. Funk, Y. Wang, Z-Q. Ma, F. A. Pereira, and N. McKenna for discussion; P. Soriano for the mouse genomic library; A. Bradley for ES cells; D. P. Edwards for the SRC-1 antibody; P. Chambon for the TIF2 cDNA; and J. D. Chen for the RAC3 cDNA. Supported by a NIH NRSA fellowship (J.X.) and NIH grants (B.W.O.).

19 November 1997; accepted 29 January 1998

Docking Phospholipase A_2 on Membranes Using Electrostatic Potential–Modulated Spin Relaxation Magnetic Resonance

Ying Lin, Robert Nielsen, Diana Murray, Wayne L. Hubbell, Colin Mailer, Bruce H. Robinson,* Michael H. Gelb*

A method involving electron paramagnetic resonance spectroscopy of a site-selectively spin-labeled peripheral membrane protein in the presence and absence of membranes and of a water-soluble spin relaxant (chromium oxalate) has been developed to determine how bee venom phospholipase A_2 sits on the membrane. Theory based on the Poisson-Boltzmann equation shows that the rate of spin relaxation of a protein-bound nitroxide by a membrane-impermeant spin relaxant depends on the distance (up to tens of angstroms) from the spin probe to the membrane. The measurements define the interfacial binding surface of this secreted phospholipase A_2.

Many interfacial enzymes such as phospholipases are water-soluble and must bind to the membrane-water interface in order to hydrolyze components of the membrane. Although the high-resolution structures of aqueous forms of several phospholipases and lipases are known (*1*), there are no reports that reveal the positioning of an interfacial enzyme at the membrane-water interface. The same can be said for most membrane-bound proteins. In the case of 14-kD secreted phospholipases A_2 ($sPLA_2$s), such as bee venom phospholipase A_2 ($bvPLA_2$), the interfacial recognition surface is thought to surround the active site slot; the latter is a deep cavity into which a single phospholipid molecule enters to reach the catalytic residues (*2*) (Fig. 1). Here we describe a high-resolution structure determination tool based on electron paramagnetic resonance (EPR) spectroscopy that allows peripheral membrane proteins such as $sPLA_2$s to be oriented with respect to the membrane-aqueous interface.

EPR methods have been developed that make use of protein site-specific spin labeling and spin relaxants for probing the membrane penetration depth of segments of integral membrane proteins that pass through the membrane (*3*). In theory developed below, it will be shown that the efficiency of relaxation of a protein-bound nitroxide spin probe by a water-soluble spin relaxant such as tris(oxalato)chromate(III) (Crox) is dependent on the positioning of the membrane with respect to the spin probe, even when the probe is exposed to the aqueous phase. By measuring the Crox-dependent relaxation of several nitroxides placed at defined locations on the surface of $bvPLA_2$, both in the presence and absence of membranes to which the enzyme binds, it is possible to position the enzyme on the membrane.

In order to apply this method to $bvPLA_2$, 13 site-selectively spin-labeled enzymes were prepared (*4*), 12 with the spin label located on or near the putative interfacial recognition surface (*1*, *2*) and 1 with the probe on the opposite side. The ability of Crox to relax the spin label of each $bvPLA_2$ mutant can be quantified by obtaining the continuous-wave EPR spectra as a function of microwave irradiation power. This series of experiments was carried out in the presence and absence of 10 mM Crox for the enzyme in the aqueous phase or bound to small unilamellar vesicles of the nonhydrolyzable, anionic phospholipid 1,2-dimyristoyl-*sn*-glycero-3-phosphomethanol (DTPM) (*5*). $bvPLA_2$ binds tightly to such vesicles (*6*). For each data set, the power dependence of the peak to peak height of the central line of the first derivative EPR spectrum, ΔY, was fit by least squares to the power saturation rollover equation (*3*, *7*)

$$\Delta Y = c\,\frac{h_1}{\left(1+\frac{(h_1)^2}{P_2}\right)^{\varepsilon}} \qquad (1)$$

where $h_1 = \alpha P_0^{0.5}$ is the microwave amplitude in gauss, P_0 is the power incident on the sample, and α is the conversion efficiency factor for the resonator (*5*) (4.5 $G/W^{1/2}$). The quantities c, ε, and P_2 were

Y. Lin and M. H. Gelb, Department of Chemistry and Department of Biochemistry, University of Washington, Box 351700, Seattle, WA 98195–1700, USA.
R. Nielsen, C. Mailer, B. H. Robinson, Department of Chemistry, University of Washington, Box 351700, Seattle, WA 98195–1700, USA.
D. Murray, Department of Physiology, State University of New York at Stony Brook, Health Science Center, Stony Brook, NY, 11794–8661, USA.
W. L. Hubbell, Jules Stein Eye Institute, Department of Chemistry and Biochemistry, University of California, Los Angeles, CA 90024–7008, USA.

*To whom correspondence should be addressed. E-mail: robinson@chem.washington.edu (B.H.R.) and gelb@chem.washington.edu (M.H.G.).